Development of a 3.2g Untethered Flapping-Wing Platform for Flight Energetics and Control Experiments

Michelle H. Rosen, Geoffroy le Pivain, Ranjana Sahai, Noah T. Jafferis, Robert J. Wood

***Abstract*— This paper presents a biologically inspired, 3.2g untethered vehicle capable of both active (flapping) and passive (gliding) flight. We discuss the overall vehicle design, as well as its validation with thrust data from benchtop testing, simulation, and flight test results. The vehicle has one pair of flapping wings for thrust generation, making it a good analogue for insects of the same scale. Flight energetics and control can be thoroughly explored through the array of simulation and testing that have been implemented. Integrated electronics provide wireless communication, sensing, and basic open-loop flight control, making flight test iteration fast and providing additional dynamics data. All of the testing setups and the physical vehicle working together have created a robust development environment for future iterations on the vehicle. The successful flight of the vehicle, including the data collection from onboard sensors and an external motion capture arena, show that this platform is ideal to study flight energetics and control schemes at an insect scale.**

I. INTRODUCTION

Small birds and insects are capable of highly efficient, highly maneuverable flight. Mimicking the performance of these fliers in robotic vehicles at an insect scale is especially challenging due to mass and size constraints, power limitations, and control for highly agile and often open-loop-unstable vehicles. However, advancements in manufacturing technologies [1], sensing [2], and control strategies [3] for flapping-wing micro-air vehicles (FWMAVs) have made the fabrication, operation, and control of such a vehicle simpler and more consistent. It is physically difficult to observe and measure flight performance, especially energetics, in an insect. A bio-inspired robotic platform may serve as an analogue to investigate various aspects of flight in a similarly sized system. For example, many large insects exhibit intermittent active (i.e. flapping) and passive (i.e. gliding, bounding, or soaring) flight. Studies indicate that this method has significant energy savings when compared to continuously flapping flight by taking advantage of the aerodynamic forces on extended wings in gliding [4]. If we take advantage of the energetics behind this flight mode, we may minimize the energy use and extend flight duration and vehicle lifespan [5]. Additionally, the insect-sized vehicle may be used for studies of sensor modalities required for autonomy and serve as a platform for under-actuated control studies and aggressive maneuvers. We have therefore developed an insect-scale robot to facilitate these studies.

In this paper, we present the development of a novel insect-scale flapping-wing micro-air vehicle. Weighing only 3.2 grams, the FWMAV has a 16-cm wingspan and carries a suite of onboard electronic systems for power, sensing, and wireless communications. We are able to easily modulate flight parameters such as the flap-glide duty cycle (ratio of time spent in active flight vs. passive flight), wing beat frequency, and full flight length for fast experiment changes. The inclusion of an inertial measurement unit (IMU) provides additional information about the dynamics of flight and moves the platform towards a fully autonomous system. Additional testing protocols have validated the thrust production, aerodynamic properties, and flight performance of the vehicle. The vehicle can therefore be used to facilitate energetics and control studies.

The authors are with the Harvard Microrobotics Laboratory, John A. Paulson School of Engineering and Applied Sciences, Harvard University, Cambridge, Massachusetts 02138, USA. Email: mrosen@seas.harvard.edu

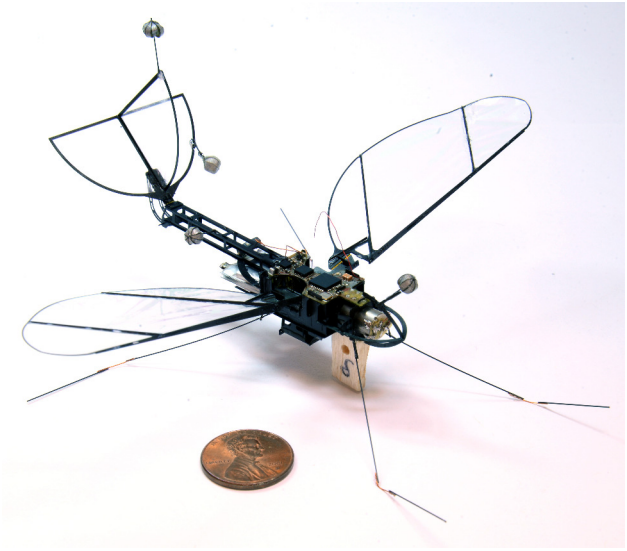

Fig. 1: 3.2g untethered flapping-wing micro-air vehicle for flight energetics and control experiments

II. VEHICLE DESIGN

Many flapping wing micro-air vehicles on the scale of large insects and small birds have been developed and successfully demonstrated flight. They range in size from the 60mg Harvard Microrobotic Fly [6] to the 19g Aerovironment NanoHummingbird [7]. These vehicles are optimized for fully active flight, especially for use in hovering, and are unable or not designed to perform passive flight. Other FWMAVs use alternative morphologies, such as a clapping wing arrangement used in the DelFly and DelFly Micro [8], [9]. An additional set of wings is used in the Georgia Tech Robot Dragonfly [10]. The vehicle presented here uses a single pair of passively rotating wings, similar to those in the Microrobotic Fly, to generate forward thrust.

TABLE I: Vehicle Mass Distribution

Component	Weight
Motor	1.217g
Transmission	140mg
Body	180mg
Wings	80mg x2
Control Board	289 mg
Batteries	377mg x2
Battery Mount	75mg
Tail	135mg
Legs	10mg x4
Vicon Markers	13mg x4
Launcher Tab	30mg
Additional Weight (wires, glue, etc.)	150mg
Total	3.22g

In addition, fixed-wing micro-air vehicles, both gliding and powered, have been developed at this scale, with careful attention given to wing planform and cross section designs. A 1.5g shape memory alloy actuated glider developed at EPFL [11] and a 2g glider developed at UC Berkeley [12] are capable of flight and control, but have no active propulsion method. The Harvard Micro-rocket Glider [13], while exhibiting passive and active flight by using micro-thrusters, does not have a biologically inspired morphology.

A FWMAV capable of both active and passive flight modes in the appropriate size range has not been previously demonstrated due to manufacturing and actuation challenges for a hybrid vehicle at this scale. This meso-scale vehicle is fully untethered, with onboard power, communication, and control systems and is capable of flapping, gliding, and ballistic flight. It is comparable in mass, wingspan, maximum flight speed, and flapping frequency to the Tobacco Hawkmoth (Manduca Sexta) [14] and can thus be considered as a rough analogue to the insect.

The vehicle consists of several independent, modular components: the body, including transmission and motor, wings with passive hinges, an adjustable angle tail, and an electronics package. Additionally, legs and reflective markers are included for flight testing. A mass breakdown of the vehicle subsystems is shown in Table I. The modularity of the vehicle makes swapping components for testing simple. The laminar fabrication process, as described in the following section, keeps performance consistent across vehicles.

A. *Body and Transmission*

The core of the robot consists of the DC motor connected to a crank-slider/slider-crank transmission. The motor, Solarbotics GM15, is the largest single component of the robot, weighing 1.2g. Because of its mass, we chose to place the motor at the front of the vehicle, to move the center of mass forward with respect to the center of lift.

The transmission design consists of a series of crank-slider to slider-cranks linkages which converts the motion of the motor into a flapping motion for the wings. The first crank-slider linkage transforms the continuous revolute motion of the motor into a linear reciprocating motion of a slider platform. This linear reciprocating motion of the slider platform then drives a pair of symmetric but mirrored slider-cranks. These symmetric cranks drive the stroke angle of the attached wings. A schematic of these linkages is shown in Figure 2a. The motion of the sliding platform is further constrained by an additional linkage that operates in a plane perpendicular to the one indicated in the schematic. This additional linkage, when paired with the symmetric slider-cranks, form a Sarrus linkage, thus ensuring linear motion of the platform. Careful attention must be given during fabrication and testing to ensure that the transmission remains symmetric.

The wings and transmission must be matched for maximum thrust production. The inertia and aerodynamic forces on the wing cause it to rotate at a certain frequency, determined by the transmission. The maximum consistent stroke-averaged thrust for the current vehicle iteration is 4g, which occurs at 25Hz, with 6.1V applied to the motor. Higher voltages drive both the motor and the batteries too hard, leading to a less efficient system that is prone to failure.

The transmission is flexure based and constructed in a 2D laminar fabrication process, as described in [1]. Individual layers of structural carbon fiber, flexible polyimide film, and heat cure adhesive are cut with a diode pulsed solid state laser before being cured with heat and pressure. Before release, the dynamic flexures of the transmission are coated with a layer of silicone (DragonSkin20 from Smooth-On) to add a spring stiffness, which increases transmission efficiency [15]. The transmission is then released and folded by hand. The outer shell of the robot is assembled around the motor and transmission using a tab-in-slot method and held in place with cyanoacrylic (CA) glue.

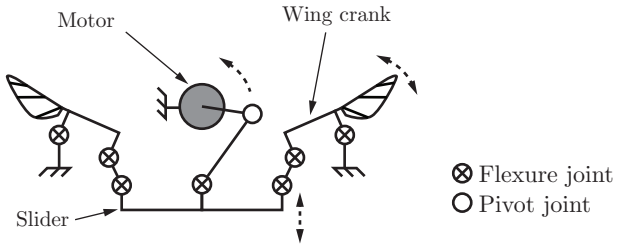

(a) Crank-slider/slider-crank transmission

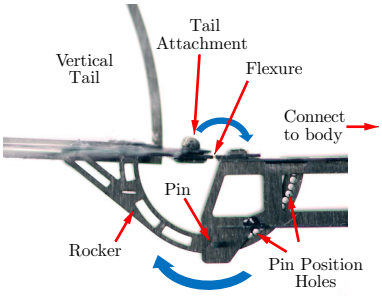

(b) Tail Mechanism

Fig. 2: Transmission and tail mechanism.

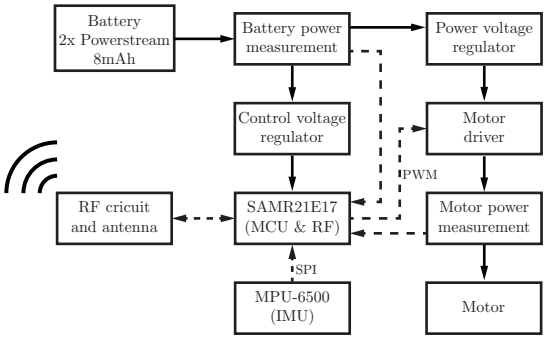

Fig. 3: Block diagram of the electronic board subsystems. Solid lines represent power, dashed lines represent data.

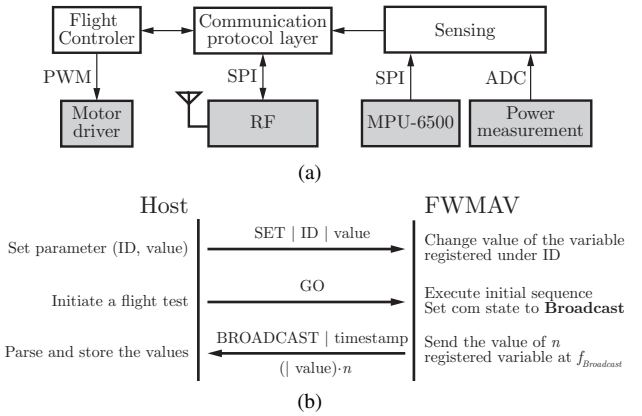

Fig. 4: (a) Interconnection between the software module and peripherals. Shaded boxes are peripherals. (b) Communication protocol. The frame structures of the communication transactions are presented on top of the arrows.

B. Wings and Tail

The wings follow a prescribed stroke pattern as determined mechanically by the transmission. A passive hinge mechanism, as described in [16], allows the wings to rotate throughout the duration of the stroke, changing the angle of attack without the need for additional actuators. The aerodynamic and inertial effects of this rotation enhances force production. While the optimal maximum wing rotation is an open research question, we use a $-45°$ to $45°$ joint stop, as it is an experimentally known good configuration for this vehicle.

The wings and tail consist of a carbon fiber structure laminated with a $2.5\mu m$ Mylar film attached using a $5\mu m$ thick double sided adhesive. Using a tiling feature of our laser micromachining system (Oxford Lasers), we are able cut an array of eight wings at a time. This ensures consistency across multiple wings. An additional support is fitted perpendicularly over the leading edge and along the wing's spars to increase flexural stiffness. This prevents unwanted torsion and greatly improves reliability.

Through simulation and vehicle flight tests, we found that changing flapping duty cycle requires adjusting the tail angle to maintain level flight, as shown in Figure 6c. We therefore require a tail that is easily adjustable between flights. A lightweight rotational mechanism was developed to allow smooth angle changes between flights as shown in Figure 2b. The tail is attached to the mount with a flexure joint, which allows the full range of angle rotation. A round rocker pulls the tail as it rotates. A small pin is inserted into one of a series of holes to maintain the angle during flight. This mechanism can be actuated in future iterations for more adaptive angle adjustment.

The vertical tail serves to stabilize the vehicle in roll and yaw. It has been demonstrated that independently controlled wings negate the need for this additional structure [17]. Our current vehicle, however, does not contain this capability, but future iterations may, allowing us to eliminate the vertical tail and approach a more bio-inspired morphology.

III. Electronics

The electronics package is composed of a single board with all necessary functions to enable wireless control and telemetry. Powered by two LiPo Powerstream 8mAh battery cells in series, the control board executes flight-tests, adjusts flying parameters, and communicates sensor data.

A. Hardware

The control system integrates an Atmel SAMR21E17 microcontroller. This system-on-chip device incorporates a radio frequency bidirectional communication peripheral (Atmel AT86RF233) and a powerful cortex M0+ microcontroller (Atmel SAMD21 core) running with an internal clock at 48MHz in a $5x5mm^2$ footprint package. The inertial measurement unit (IMU) InvenSens MPU-6500 measures the rotation rates and accelerations in the body-fixed coordinate frame.

In addition to the IMU, the control board also includes sensors to monitor the battery and motor power consumption. This enables an estimation of the electrical efficiency of the FWMAV, which is given by

$$\eta = P_{\text{motor}}/P_{\text{battery}} \tag{1}$$

Additionally, knowing the state of the batteries helps avoid damage, which is particularly relevant to this FWMAV given the high anticipated C-rates. The vehicle will not turn on the motor if the battery charge is below a set voltage.

Two high efficiency ($\sim 80\%$) switching voltage regulators were chosen to condition the voltage supplied by the batteries for the control and power electronics. Pulse width modulation (PWM) is used to drive the motor, enabling us to vary the set of experimental flight parameters such as the flap-glide period and duty cycle, wing beat frequency, and total duration of flight.

B. Integration

The electronic board is shaped to mount directly on the body of the vehicle. The circuit is a double-sided polyimide-based flex PCB that is manufactured in-house. The control module sits on top of the vehicle and is connected via a ribbon cable to the power module on the back panel. To prevent shorting of the traces, the top and back body panels

are coated in an approximately $5\mu m$ thick layer of non-conductive CVD Parylene.

The batteries are mounted on the back of the robot and serve as an additional structural support for the tail. The batteries are connected and disconnected from the board using a set of two small header pins and sockets. This design allows the batteries to be charged without needing to remove them from the robot.

C. Software

The software integrates three main modules: sensing, flight control, and communication. The sensing module, which runs through software interrupts, gathers sensor information as a background task. An update rate of 1kHz for the IMU data and 15kHz for the power data is observed.

The simple flight controller module implements basic control of the vehicle. It currently uses an open-loop control strategy to provide wing actuation based on pre-set flight parameters. Future vehicle iterations will include state estimation, more advanced control, and control surfaces to facilitate autonomous control.

The communication protocol layer allows a simple bidirectional interaction through the RF peripheral to set flight parameters and record telemetry data. The communication module sends the telemetry values at a data rate of up to 390Hz during the flight. This is roughly an order of magnitude faster than the flapping frequency. A timestamp is added to the telemetry to synchronize the collected data with the off-board measurement systems. To save bandwidth, the structure of the broadcast frame, order, type and number of values, are preset by the experimenter on the host and on the vehicle.

IV. Testing

A. Thrust and Aerodynamics

To validate the thrust production of the vehicle, we use a dedicated force sensor test setup. The vehicle is mounted nose-down on a Nano 17 Titanium 6-axis force/torque sensor (ATI Industrial Automation) and the wings are actuated. Stroke average forces and torques are recorded for various input voltages which correspond to varying flapping frequencies. A high speed camera mounted above the vehicle captures the wing motion. This is used to monitor and debug the time evolution of the wing stroke and rotation angles. Though the wings get close to the sensor platform at the bottom of their stroke, we have experimentally determined that this does not greatly impact our overall thrust measurements. However, we choose the lowest measured value to ensure that the vehicle has more thrust than weight in case of any measurement errors. In developing a flight-worthy vehicle, aerodynamic forces on the body must also be considered. To this end, we use a low-speed wind tunnel to experimentally determine the lift and drag coefficients at various angles of attack as shown in Figure 5a. For overall body aerodynamics in glide, the FWMAV is mounted on the end of a long moment arm connected to a Nano 17 Titanium force/torque sensor. This assembly is attached to a rotation stage to sweep through angles of attack. The wind speed is varied from $1m/s$ to $5m/s$ More detail on this setup can be found in [5].

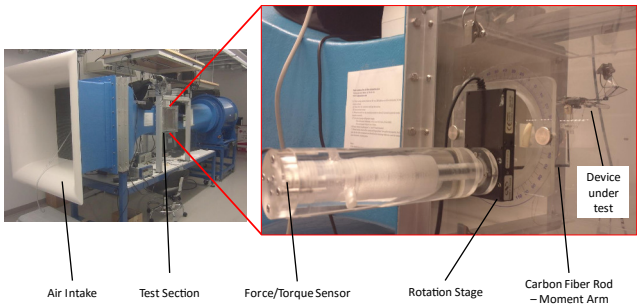

(a) Low-Speed Wind Tunnel

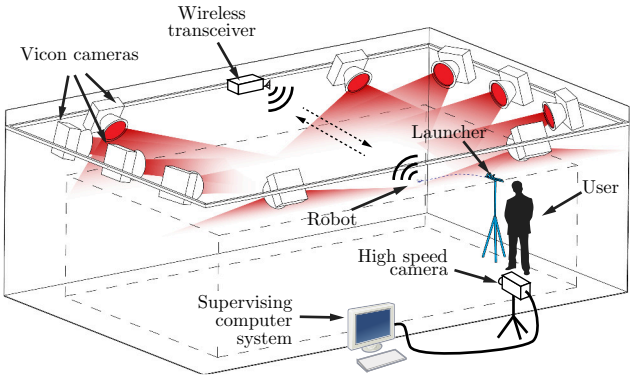

(b) Flight Arena

Fig. 5: Wind tunnel and Vicon flight arena.

B. Flight Experiment Setup

The vehicle is flown in a motion capture arena with ten Vicon T-series cameras, as shown in Figure 5b. The system tracks the position and orientation of the flier using lightweight infrared reflective markers. The markers are placed in such a way that at least three are visible from all angles during a flight. The system captures data at 100Hz, much faster than the dynamics of the vehicle, which occur at 8-10Hz. A wireless transceiver is mounted on the ceiling of the arena to communicate with the vehicle in flight.

The MAV is launched from a custom made launcher shown on the right in Figure 5b. The vehicle is placed on the shuttle and jaws are locked in place to grip it. Copper contacts on the bottom of the jaw touch, indicating to the overall system that the robot is in place. The shuttle is pulled back along the rail and released to give the vehicle an initial velocity. We can adjust the initial launch angle by tilting the platform and can adjust the velocity by changing the stiffness of the spring connecting the shuttle to mechanical ground. The latch is pushed open by a wedge at the front of the launcher and the spring-loaded jaws open, releasing the vehicle. The copper pads are no longer in contact, signaling the moment of launch to the data collection system and to the microcontroller.

The full experimental setup is coordinated by an xPC Target real time operating system. The Vicon system streams orientation and position data through a serial port to the target, where it is parsed and filtered in real time. The

system also watches for the change in launcher signal, which indicates the start of a flight. This signal change also triggers the vehicle to begin flapping. A Phantom Miro high-speed camera collecting data at 500 fps is triggered by the system at the experiment start. The data is collected and organized into a readable format at the end of a test.

Communication with the vehicle is enabled as soon as the battery is connected. Therefore, the vehicle is placed in the launcher jaws before the power is connected. The start of the experiment software sends the flight parameter data to the vehicle. On launch, it starts flapping in the predetermined pattern and streams the data gathered by its sensors. The synchronization of the launch signal and the start of flapping ensures that the start of the flight is consistent across tests. At the end of the flight, the collected sensor data is parsed and plotted. A full flight experiment takes only five minutes, including data processing, and can be run by a single experimenter.

V. Simulation

The data from thrust testing, wind tunnel aerodynamic testing, and preliminary flight tests was used to create a 6 degree-of-freedom simulation of the flight vehicle in three-dimensional space. This simulation was used to tune the parameters of the vehicle, including tail angle, tail size, and component placement. For a fixed vehicle design, the tail angle is the most easily adjusted, so here we describe a longitudinal dynamics simulation for determining tail angle to achieve level flight for a given duty cycle.

The equations of motion are derived using a traditional fixed-wing aircraft formulation with Newtonian mechanics. Twelve state variables are solved at each time step. Global position is denoted as (X,Y,Z) and the body-fixed velocity given by (v_x,v_y,v_z). The orientation of the body is given by the Euler angles (Φ,Θ,Ψ) in the global frame. The angular velocities (p,q,r) are represented in the body frame. The complete free body diagram is shown in Figure 6a.

The main body and tail are treated as independent bodies so that the tail angle may be varied easily, separate from the body. The lift and drag coefficients of the body and tail are taken from wind tunnel experiments. We simplify the model by ignoring the aerodynamic contributions of the control board and batteries. The board is fully integrated into the vehicle body and is low profiled, while the batteries sit in the wake of the vehicle. The mass of the legs, markers, and other additional mass are included in the mass of the body.

The flapping thrust force is modeled simply as a sinusoidal input with the stroke-averaged force as measured by our bench-top tests. This force may be rotated slightly with respect to the horizontal plane of the body (Φ_{thrust}), creating components in both lift and thrust. For a thrust force of 4g at a frequency of 25Hz, the force is given by

$$F_{Thrust} = (0.1\sin(2\pi\times 25t)+0.04)\begin{bmatrix}\cos\Phi_{Thrust}\\0\\\sin\Phi_{Thrust}\end{bmatrix} \quad (2)$$

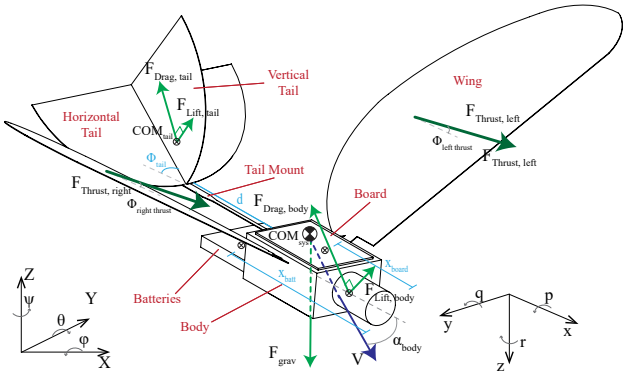

(a) 3D simulation model, including state variable definitions. Light blue parameters are varied to achieve a more optimized flight.

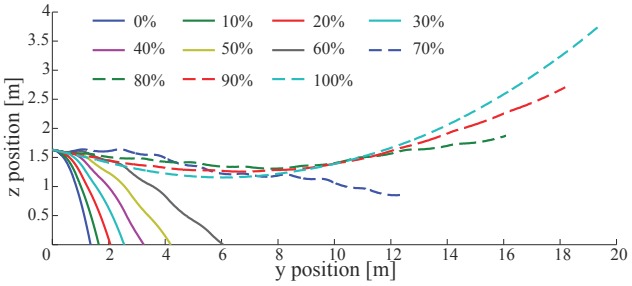

(b) Simulated 3 second flights across duty cycles, optimized with ideal tail angle.

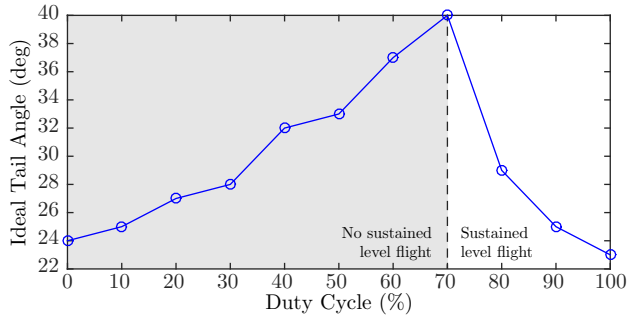

(c) Optimized tail angle as a function of duty cycle.

Fig. 6: Simulation setup and results

placed at the quarter chord of the wing. This simplified representation has been successful in modeling the high-level behavior of the vehicle. Further refinement of the model, however, will include a more accurate representation of the transmission and aerodynamic effects on the wings.

The simulation is able to vary several geometric parameters, including the position of the center of mass of the board and batteries, the distance between the body and tail, and the tail angle. Thus, we are able to perform pre-flight simulations with varying parameters which are used to trim the vehicle. This reduces the number of necessary flights, prolonging the life of the robot.

In Figures 6b and 6c, we present an example of flight optimization for various duty cycles with respect to tail angle. Simulations were run for tail angles varying from 0 deg to 90 deg for each duty cycle. The flight traveling the farthest

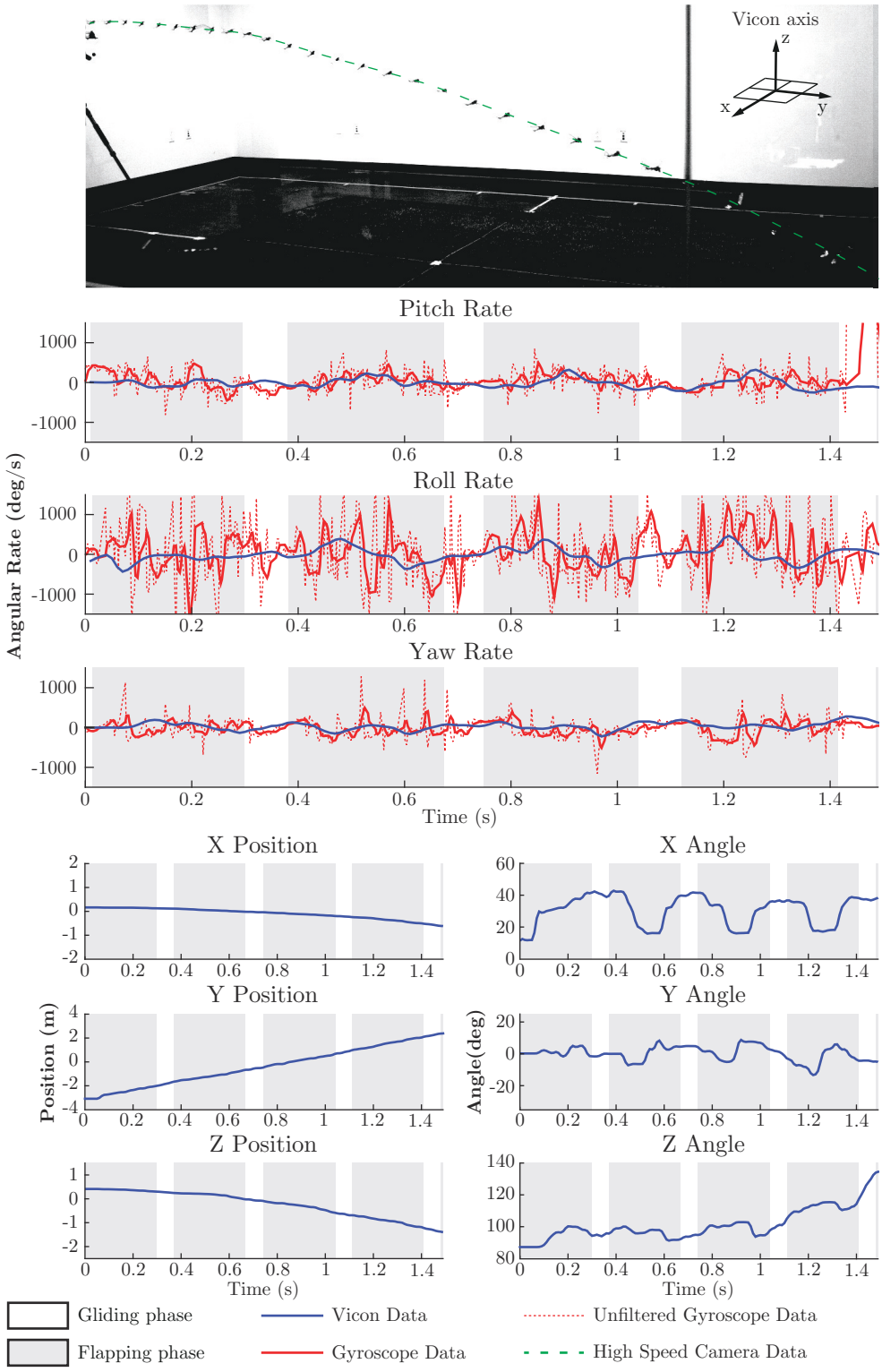

Fig. 7: Combined results and data from 80% duty cycle flight experiments.

horizontal distance was selected as the optimal flight. We notice that below a 70% duty cycle, the vehicle is unable to sustain level flight, regardless of tail angle. This corresponds to a change in the plot of optimal tail angle versus duty cycle in Figure 6c.

VI. Results

With the incorporation of results from both the experimental tests and trimming information from the simulation, the vehicle was able to perform a series of stable flights. The data from these flights was captured by the Vicon system, the high speed camera, and the on-board sensors simultaneously. A sample of the data from a successful flight is presented in Figure 7. The high speed camera records at 500Hz, and is sampled here at 20Hz. The Vicon samples at 100Hz and the IMU samples at an average of 390Hz.

The Vicon data is filtered with a second order lowpass Butterworth filter with a cutoff frequency of 30Hz. This ensures that we see both body dynamics and the effects of flapping on the data. However, we find that the Vicon data is highly unreliable. The system has trouble tracking the vehicle, as the markers are very small compared to the arena size, the vehicle moves quickly. The vibration of the body and tail due to the flapping wings also has an effect. We implemented a median filter to eliminate spikes in the data, occurring from occlusion of the markers. The Vicon data is thus only able to give a general trend of the motion, rather than resolving the faster dynamics.

The gyroscope data is able to capture higher order modes. We filter the raw data with a second order lowpass Butterworth filter with a cutoff frequency of 50Hz. This allows us to see the body dynamics, flapping effects, and the higher order dynamics present at 50Hz while eliminating noise. The gyroscope provides significantly more information about the vehicle motion than the Vicon. This additional data can be used to learn more about the vehicle dynamics, as well as being used for control and state estimation in the future. Successful control of a FWMAV with data from this IMU has been demonstrated in [2].

VII. Future Work

We have developed and validated a lightweight flapping-wing vehicle for conducting energetics studies. The robot is able to easily modulate the duty cycle for various flight experiments. It also successfully collects movement data from integrated sensors and streams it wirelessly. Further aerodynamic optimization will be pursued.

With the data from the IMU, we will be able to estimate the orientation state of the robot. We can therefore remove the FWMAV from the Vicon arena and fly it in bigger, less constrained spaces. We also plan to use the IMU data to implement a closed-loop control scheme to maintain level and straight flight. Additionally, actuated control surfaces will be added to the tail, as well as the ability to adjust the tail angle in flight. This gives us the ability to perform more complex maneuvers, as well as stabilize the vehicle. A split-wing design, where the wings are flapped independently, is also a future possibility for greater control authority.

Acknowledgments

The authors thank the members of the Harvard Microrobotics Lab and the Wyss Institute for Biologically Inspired Engineering for helpful discussions, assistance, and support. This work is partially funded by the Wyss Institute for Biologically Inspired Engineering and the National Science Foundation Graduate Research Fellowship (Grant No. DGE1144152). Any opinion, findings, and conclusions or recommendations expressed in this material are those of the authors and do not necessarily reflect the views of the National Science Foundation.

References

[1] J. P. Whitney, P. S. Sreetharan, K. Y. Ma, and R. J. Wood, "Pop-up book mems," *Journal of Micromechanics and Microengineering*, vol. 21, 2011.

[2] E. Helbling, S. Fuller, and R. Wood, "Pitch and yaw control of a robotic insect using an onboard magnetometer," *IEEE International Conference on Robotics and Animation*, 2014.

[3] K. Ma, P. Chirarattanon, S. Fuller, and R. J. Wood, "Controlled flight of a biologically inspired, insect-scale robot," *Science*, vol. 340, pp. 603–607, 2013.

[4] B. W. Tobalske, "Biomechanics of bird flight," *Journal of Experimental Biology*, vol. 210, pp. 3135–3146, 2007.

[5] M. Kovac, D. Vogt, D. Ithier, M. Smith, and R. J. Wood, "Aerodynamic evaluation of four butterfly species for the design of flapping-gliding robotic insects," *IEEE/RSJ Int. Conf. on Intelligent Robots and Systems*, 2012.

[6] R. J. Wood, "Design, fabrication, and analysis of a 3dof, 3cm flapping-wing mav," *IEEE/RSJ International Conference on Intelligent Robots and Systems*, 2007.

[7] M. Keennon, K. Klingebiel, H. Won, and A. Andriukov, "Development of the nano hummingbird: A tailless flapping wing micro air vehicle," *50th AIAA Aerospace Sciences Meeting*, 2012.

[8] C. D. Wagter, S. Tijmons, B. Remes, and G. de Croon, "Autonomous flight of a 20–gram flapping wing mav with a 4–gram onboard stereo vision system," *IEEE Int. Conf. on Robotics and Automation*, 2014.

[9] G. C. H. E. de Croon, K. M. E. de Clerq, R. Ruijsink, B. Remes, and C. de Wagter, "Design, aerodynamics, and vision–based control of the delfly," *International Journal of Micro Air Vehicles*, vol. 1, pp. 71–97, 2009.

[10] J. Ratti and G. Vachtsevanos, "A biologically–inspired micro aerial vehicle: Sensing, modeling and control strategies," *Journal of Intelligent and Robotic Systems*, vol. 60, pp. 153–178, 2010.

[11] M. Kovac, A. Guignard, J.-D. Nicoud, J.-C. Zufferey, and D. Floreano, "A 1.5g SMA–actuated microglider looking for the light," *IEEE International Conference on Robotics and Automation*, 2007.

[12] R. J. Wood, S. Avadhanula, E. Steltz, M. Seeman, J. Entwistle, A. Bachrach, G. Barrows, S. Sanders, and R. S. Fearing, "An autonomous palm-sized gliding micro air vehicle," *IEEE Robotics and Automation Magazine*, 2007.

[13] M. Kovac, M. Bendana, R. Krishnan, J. Burton, M. Smith, and R. J. Wood, "Multi–stage micro rockets for robotic insects," *Robotics: Science and Systems*, 2012.

[14] R. D. Stevenson, K. Corbo, L. B. Baca, and Q. D. Le, "Cage size and flight speed of the tobacco hawkmoth manduca sexta," *Journal of Experimental Biology*, vol. 198, pp. 1665–1672, 1995.

[15] R. Sahai, K. C. Galloway, and R. J. Wood, "Elastic element integration for improved flapping–wing micro air vehicle performance," *IEEE Transactions on Robotics*, vol. 29, 2013.

[16] J. Whitney and R. Wood, "Aeromechanics of passive rotation in flapping flight," *Journal of Fluid Mechanics*, vol. 660, pp. 197–220, 2010.

[17] A. A. Paranjape, S.-J. Chung, and M. S. Selig, "Flight mechanics of a tailless articulated wing aircraft," *Bioinspiration and Biomimetics*, vol. 6, 2011.